Top Catal (2016) 59:506–515
DOI 10.1007/s11244-015-0521-7

ORIGINAL PAPER

Oxidation of Ultrathin FeO(111) Grown on Pt(111): Spectroscopic Evidence for Hydroxylation

Niclas Johansson[1] · Lindsay R. Merte[1,2] · Elin Grånäs[1] · Stefan Wendt[2] · Jesper N. Andersen[3] · Joachim Schnadt[1] · Jan Knudsen[3]

Published online: 6 January 2016

Abstract Using high resolution and ambient pressure X-ray photoelectron spectroscopy we show that the catalytically active FeO_2 trilayer films grown on Pt(111) are very active for water dissociation, in contrast to inert FeO(111) bilayer films. The FeO_2 trilayer is so active for water dissociation that it becomes hydroxylated upon formation, regardless of the applied preparation method. FeO_2 trilayers were grown by oxidation of FeO(111) bilayer films either with molecular oxygen in the mbar regime, or by NO_2 and atomic oxygen exposures, respectively, in the ultrahigh vacuum regime. Because it was impossible to prepare clean FeO_2 without any hydroxyls we propose that catalytically highly active FeO_2 trilayer films are generally hydroxylated. In addition, we provide spectroscopic fingerprints both for Pt(111)-supported FeO(111) and FeO_2 films that can serve as reference for future in situ studies.

Keywords Spectroscopy · Iron oxide monolayers · Ultrathin films · Hydroxylation

✉ Jan Knudsen
jan.knudsen@sljus.lu.se

[1] Division of Synchrotron Radiation Research, Department of Physics, Lund University, Box 118, 221 00 Lund, Sweden

[2] Interdisciplinary Nanoscience Center (iNANO) and Department of Physics and Astronomy, Aarhus University, 8000Aarhus C, Aarhus, Denmark

[3] Division of Synchrotron Radiation Research and the MAX IV Laboratory, Department of Physics, Lund University, Box 118, 221 00 Lund, Sweden

1 Introduction

The ultrathin FeO(111) bilayer film grown on Pt(111) is one of best studied hetero-oxide hybrid system that couples a subnanometer sized oxide phase to a metal surface [1]. It was first grown and characterized in 1988 by Vurens et al. [2] Since then the FeO(111) bilayer film on Pt(111) has been characterized in great detail using the combination of scanning tunneling microcopy (STM) and low energy electron diffraction (LEED) [3–7], X-ray photoelectron diffraction [8], and density functional theory (DFT) [7, 9, 10]. From these studies it is known that the FeO(111) bilayer consist of hexagonal closed packed O- and Fe-layers with the O-layer at the surface and the Fe-layer sandwiched between the surface O-layer and the Pt(111) support. Due to a small misfit angle (0.6°) between the FeO(111) film and the Pt(111) support and the lattice mismatch between the FeO lattice ($\sim$ 3.1 Å) and the Pt(111) substrate (2.77 Å) a characteristic moiré pattern with a $\sim$ 25 Å periodicity is formed.

Numerous interesting properties of the FeO(111) films have been discovered in various studies that focused on: (i) the reduction of the film by atomic hydrogen [11–13]; (ii) reduction of the film by CO [14]; (iii) nanopattering using the films moiré structure [15–18]; (iv) adsorption of molecules on the film [5, 19–22]; and (v) catalytic activity of the film [23, 24].

One of the reactivity studies published by Sun et al. in 2009 [23] revealed that an oxygen-rich FeO_x ($1 < x < 2$) trilayer phase is formed when FeO(111) bilayer films are exposed to O_2 pressures in the mbar regime at elevated temperatures. The formation of this oxygen-rich FeO_x phase at reaction conditions was linked to the enhanced CO oxidation activity observed for ultrathin FeO(111) as compared to clean Pt(111) and nm-thick Fe_3O_4(111). In the

following, the O-enriched FeO_x phase will be referred to as FeO_2 trilayer. Since its discovery, the FeO_2 trilayer phase has been studied extensively by a variety of techniques, including STM [25–28], Auger electron spectroscopy (AES) [25], and DFT [26, 29, 30]. In a study by Giordano et al. [10] it was shown that the transition from FeO(111) to FeO_2 strongly depends on the specific region, leading to oxygen enrichment in specific areas of the FeO(111) moiré unit cell. In addition, it was shown that the FeO_2 trilayer islands have a O–Fe–O–$Pt_{substrate}$ stacking. Compared with the FeO(111) bilayer film, the FeO_2 islands thus contain O atoms at the interface between the oxide film and the Pt(111) substrate. Finally, high resolution STM studies revealed a $(\sqrt{3} \times \sqrt{3})R30^\circ$ superstructure on the FeO_2 trilayer islands. On the basis of DFT calculations it was suggested that this superstructure originates from a energetically preferred location of O-interphase atoms atop the Pt atoms of the substrate [10]. In two more recent studies by Giordano et al. [29, 30] theoretical core level shifts (CLS's), work function changes between FeO(111) and FeO_2, and OH stretching frequencies were reported and the mapping of the local activity at different sites showed that oxygen easily can be adsorbed and released at the FeO(111)/FeO_2 boundaries, which might explain the high CO oxidation activity. Studies by Lewandowski et al. [27] showed (i) that the FeO_2(111) phase is also formed on Pt particles supported on Fe_3O_4(111) upon annealing in O_2 in the mbar pressure range, and (ii) that CO_2 formation occurs via a Mars-van Krevelen mechanism, where CO reacts with the FeO_2 trilayer film, thereby reducing it, while O_2 oxidizes FeO back to FeO_2 [28]. This proposed mechanism by Lewandowski et al. fits well with the reaction mechanism proposed in the DFT study by Giordano et al. [30] All the studies addressing the FeO_2 trilayer mentioned above considered the formation of FeO_2 by O_2 and its reduction by CO. However, a recent study by Ringleb et al. demonstrates that hydroxylated FeO_2 can be formed from FeO(111) if H_2O and O_2 are dosed simultaneously at near ambient pressure, leading to a H-O-Fe-O-$Pt_{substrate}$ structural motive [31].

Indeed, a lot of efforts have been devoted in determining the topology, local electronic structure, and reactive sites of FeO_2 trilayer films using STM and DFT. However, spectroscopic information on the electronic structure of FeO_2 films is still lacking. Solely the study by Ringleb et al. [31] reports on X-ray photoelectron spectroscopy (XPS) data, but in this study the FeO_2 surface was intentionally hydroxylated, as it was produced by co-dosing of O_2 and H_2O onto a FeO(111) bilayer film.

Here we present a spectroscopic investigation of the FeO_2 trilayer film grown on Pt(111). We report XPS and X-ray absorption spectroscopy (XAS) fingerprints for bilayer FeO(111) and trilayer FeO_2. The FeO_2 trilayer films were formed by oxidizing FeO(111) either with molecular oxygen in the mbar regime or with NO_2 and atomic oxygen, respectively, dosed in the ultrahigh vacuum (UHV) regime. Independent of the preparation method we observe spectroscopic evidence for a significant degree of hydroxylation on the FeO_2 trilayer films, and our STM data are fully consistent with this conclusion. Ambient pressure X-ray photolectron spectroscopy (APXPS) measurements conducted while oxidizing FeO(111) to FeO_2 further reveals that the onset and degree of hydroxylation correlate with the coverage of FeO_2 trilayer islands. Altogether, our observations are strong evidence for an astonishing high activity of the FeO_2 trilayer towards water dissociation. Furthermore, our experimental data suggest that Pt(111)-supported FeO_2 trilayer films are generally hydroxylated, regardless of the applied preparation recipe.

2 Experimental

High resolution X-ray photoelectron spectroscopy (HRXPS) and XAS in UHV were performed at beamline I311 of the MAX IV Laboratory in Lund, Sweden. The beamline as well as the endstation are described in detail elsewhere [32]. High-pressure experiments in the mbar range were performed at the APXPS endstation of beamline I511. The APXPS instrument is capable of performing in situ experiments in pressures up to ~ 5 mbar in a dedicated reaction cell inside the main analysis chamber. A description of the instrument and the beamline can be found in refs. [33] and [34], respectively.

In the HRXPS and the APXPS experiments, the Pt(111) crystal was cleaned by repeated cycles of Ar^+ sputtering followed by annealing to 870 K in 1×10^{-7} mbar O_2. After annealing the crystal was subsequently flashed to 970 K. The cleanness of the crystal was probed by LEED and XPS. To grow the FeO(111) bilayer film, Fe was deposited onto Pt(111) with an e-beam evaporator. The deposited Fe was oxidized by heating the crystal to 870 K in $1 \cdot 10^{-6}$ mbar O_2. This procedure is known to result in a FeO(111) bilayer film, which grows layer-by-layer up to a coverage of about 2.5 ML [4]. The coverage of the FeO film in the XPS experiments was calibrated by saturating the surface with CO at room temperature. As CO only binds to the exposed Pt surface at room temperature the intensity of the C 1s and O 1s signal can be used directly to follow the growth of the film. By cycles of Fe deposition (submonolayer amounts) at room temperature and subsequent oxidation, we tuned the coverage of FeO to the point where the C 1s signal disappeared. We define a monolayer (ML) as a complete coverage of a bilayer FeO(111) film, noting

that the FeO(111) lattice is expanded by about 12 % [13] resulting in 0.8 layer coverage with respect to the Pt(111) surface density. All sample temperatures given in our work are measured with a type K thermocouple spot-welded to the edge of the Pt(111) single crystal surface. In the APXPS experiments we used O_2 (99.9999 % purity) without further purification. The base pressure of the APXPS chamber was $\sim 5 \times 10^{-10}$ mbar. In the HRXPS measurements performed at beamline I311 we used NO_2 (99.5 % purity) for the oxidation. The NO_2 was dosed at a maximum pressure of 1×10^{-7} mbar at room temperature. No filaments were on during NO_2 exposure and a cold cathode gauge was used to measure the pressure when NO_2 was dosed. The base pressure of the HRXPS setup was $\sim 1 \times 10^{-10}$ mbar. The XPS spectra shown in this paper are calibrated to the Fermi level. All O 1s spectra were acquired using a photon energy of 650 eV. In our experiments, this yields a resolution of 580, 950 and 250 meV for UHV, mbar and NO_2 experiments, respectively. The Pt 4f and Fe 3p/Pt 5p regions were recorded with a photon energy of 190 eV, yielding corresponding resolutions of 110 meV for the Pt 4f and 330 meV for the Fe 3p/Pt 5p levels. Polynomial backgrounds were subtracted from all spectra before or during the curve fitting. For Pt 4f spectra Doniach-Šunjić (DS) functions convoluted with Gaussians line shapes were used for the curve fitting. O 1s spectra were deconvoluted using asymmetric Voigt functions. Due to the open-shell nature of Fe, fitting of Fe 3p features is non-trivial. For simplicity we used three DS components convoluted with Gaussians for curve fitting of the Fe 3p features.

The Fe L-edge XAS spectra were recorded in normal incidence in Auger yield mode by collecting electrons with a kinetic energies between 540 and 550 eV using a SES-200 analyzer. The photon energy of the XAS spectra was calibrated by measuring the Pt 4f peak using first and second order light from the monochromator.

STM measurements were conducted in a separate UHV system in Aarhus with a base pressure of $\sim 2 \times 10^{-10}$ mbar, using a home-built Aarhus STM operated at room temperature with a mechanically cut Pt–Ir tip. Preparation of the Pt(111) crystal and growth of the FeO film were conducted in the same way as for the spectroscopy measurements. To form the FeO_2 trilayer, the bilayer FeO(111) film was exposed to atomic oxygen at 385 K using a thermal atom source (Oxford Applied Research TC-50) operated at a power of 54 W with a chamber background O_2 pressure of 2×10^{-8} mbar. Exposure for 8 min under these conditions followed by flash annealing to 500 K was found to produce a film that was nearly saturated with FeO_2 trilayer islands, similar to a previous study of the oxidation of FeO/Pd(111) [35] conducted using the same experimental system.

3 Results and Discussion

The spectroscopic and structural properties of Pt(111)-supported FeO(111) bilayer films are well documented in the literature [5, 13]. Nevertheless, to facilitate a direct comparison of the XPS data acquired on FeO_2 we first show the spectra of clean Pt(111) surface (top Fig. 1) and the bilayer FeO(111) film (middle Fig. 1). Subsequently, the spectroscopic and structural properties of FeO_2 will be discussed. Ball models and LEED images for the different preparation steps are also shown in Fig. 1.

3.1 Spectroscopic Fingerprints of FeO

Before growing of the FeO(111) film the spectral features corresponding to a clean Pt(111) surface is discussed. No signal is observed in the O 1s region. In the Pt $4f_{7/2}$ line bulk (Pt_B) and surface (Pt_S) components are observed at 70.94 and 70.52 eV [36], respectively. The small component observed at 51.40 eV originates from the Pt 5p core level of the clean Pt(111) surface. Following the growth of 1 ML FeO(111) a single O 1s peak is observed at 529.4 eV (denoted I). In the Pt $4f_{7/2}$ region the previously observed surface component disappears and one single component is observed at 70.94 eV, i.e. the position of the bulk component of the Pt(111). The CLS of the topmost layer of Pt atoms that binds to Pt atoms beneath and Fe atoms above is thus indistinguishable from that of the Pt bulk atoms. In the Fe 3p region a component with first moment—i.e. 'center of mass'—at 54.99 eV and peak maximum at 54.11 eV is observed. The spectra acquired here on FeO(111) are in good agreement with those published previously [5, 13]. The cleanliness of our FeO(111) films was further confirmed by acquiring survey scans, which showed no sign of the presence of other elements than Fe, O, and Pt. The ordering of the film was checked with LEED, which revealed the expected floret patterns due to the film's moiré structure (see the insets in Fig. 1). Careful inspection of the individual diffraction spots reveal an arc shape that could indicate the formation of slightly rotated FeO(111) domains on the sample. Most likely a higher oxidation temperature after iron deposition would have given sharp spots without any arc shape.

3.2 Spectroscopic Fingerprints of FeO_2

For the formation of the FeO_2 trilayer film the FeO(111) film was oxidized by dosing 0.6 mbar O_2 while annealing

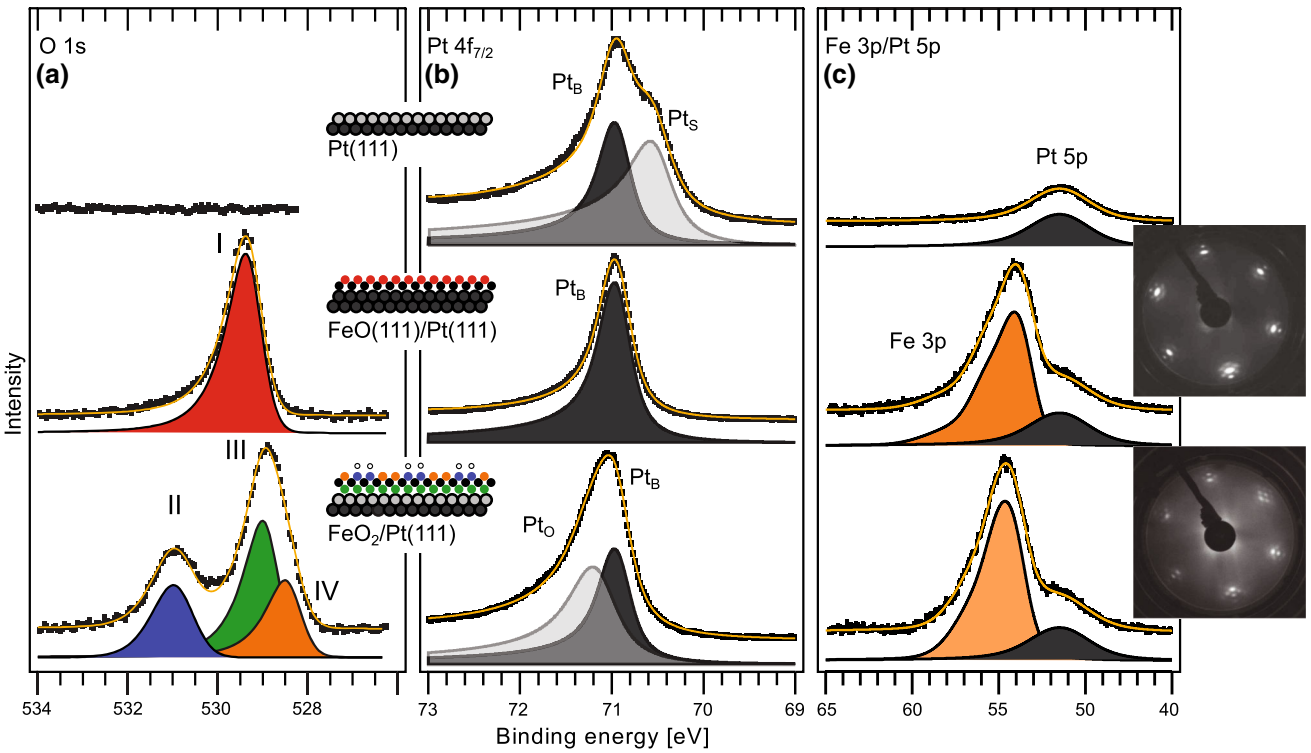

Fig. 1 XP spectra acquired on the clean Pt(111) crystal (*top*), with a bilayer FeO(111) overlayer (*middle*), and with a trilayer FeO_2 overlayer (*bottom*). *Panel a* shows the O 1s core levels, while *panels b, c* show Pt $4f_{7/2}$ and Fe 3p/Pt 5p regions, respectively. LEED images of FeO(111) and FeO_2 overlayers acquired in the XPS setup with energies of 62 and 65 eV, respectively, are also included in the figure.

the sample at 500 K. Subsequently the sample was cooled to room temperature in an oxygen atmosphere. Following the oxidation, the main O 1s peak shifts to lower binding energy and a shoulder component develops at the high binding energy side. The full width at half maximum (FWHM) of the main O 1s peak of the FeO_2 trilayer film is significantly larger (1.1 eV) than the FWHM of the O 1s component (I) observed on the bilayer FeO(111) (0.9 eV) suggesting that more than one component should be used for its deconvolution. On the basis of this observation we fitted the main O 1s peak by two components with similar widths as component I positioned at 529.0 eV (III) and 528.5 eV (IV), respectively. Our experimental CLS of −0.4 eV (III) and −0.9 eV (IV) with respect to component I of FeO(111) agree very well with DFT-calculated final state CLS of −0.4 eV (interface O) and −0.7 eV (surface O) reported by Giordano *et al.* [29] Accordingly, we assign component III to interface O atoms sandwiched between Pt and Fe atoms and component IV to surface O atoms in FeO_2.

The shoulder component (II) located at 531.0 eV is shifted by +2.5 eV with respect to component IV originating from surface O atoms in FeO_2. Core-level shifts of ∼2 eV have previously been observed for hydroxylation of oxide films such as FeO(111) (2.2 eV) [13], Fe_3O_4(111) (2.1 eV) [37], α-Al_2O_3(0001) (1.9–2.0) [38], and α-Fe_2O_3(0001) (1.9–2.2 eV) [38]. On this basis we assign the shoulder component (II) to OH groups. Comparing the relative area of the OH component II (49%) and the FeO_2 surface component IV (51%) we conclude that approximately half of the surface O atoms in the FeO_2 film are hydroxylated. However, it should be noted that the area of component IV is very sensitive to the peak widths of component IV and III. Thus, the real coverage of OH-groups could easily be higher or lower than 0.5 ML.

In contrast to the FeO(111) film, the FeO_2 trilayer film contains interface O atoms in direct contact with the topmost layer of Pt atoms. Therefore, we expect the Pt $4f_{7/2}$ spectra of FeO(111) and FeO_2(111) to be clearly distinguishable. Figure 1b confirms this expectation as we find a new component (Pt_O) at 71.15 eV binding energy in addition to the bulk component (Pt_B) at 70.94 eV for the FeO_2(111) film. For comparison, ref. [36] reported a Pt $4f_{7/2}$ binding energy of 71.12 eV for a p(2 × 2)-O chemisorption phase on Pt(111) with O atoms located in the threefold hollow sites.

In the Fe 3p spectrum the oxidation of FeO(111) to FeO_2 causes a CLS of +0.53 eV of the Fe 3p component peak

maximum, suggesting a higher oxidation state of Fe in the FeO_2 film. However, the CLS causes only the first moment to shift by +0.18 eV. Hence, the overall peak has shifted possibly due to multiple changes on the surface. We did not attempt to explicitly curve fit the Fe 3p peak since both the Fe 2p and 3p curve fitting are non trivial [39–41] and beyond the scope of the present study. Instead we used three Doniach-Šunjić (DS) functions to fit the Fe 3p peak in order to determine the integrated area. In Fig. 1c the sum of these three DS functions is plotted as one component shown in orange. By normalizing the spectra to the integrated area of the Pt 5p component we observe a 13 % increase of the Fe 3p component upon oxidation from FeO(111) to FeO_2, fitting well with the fact that more attenuation of the photoelectrons from underlying Pt is expected for FeO_2 than for FeO(111).

Finally, we note that also the LEED pattern acquired on FeO_2 shows a floret pattern, similar to the one observed on the FeO(111) film, but without any arc shape of the individual diffraction spots. First of all this indicates that the in-plane structures of the FeO(111) and FeO_2 surfaces are comparable even though the spectroscopic fingerprints of these two surfaces are very different. Secondly, the disappearance of the arc shape upon FeO_2 formation might be an indication that rotational micro domains disappeared upon oxidation when the interphase O layer became present. Note that the two LEED images shown in Fig. 1 are acquired on the the same sample before and after FeO_2 formation. More experimental work and a careful analysis of many LEED images before and after oxidation are, however, needed to verify our second conclusion.

As mentioned above, our O 1s deconvolution indicates that approximately 50 % of the surface oxygen atoms are hydroxylated. To validate this conclusion we tried to selectively remove the H atoms from the surface, by flashing the FeO_2 trilayer to 580 K. In Fig. 2 we compare the O 1s spectrum of FeO_2 before (bottom) and after (middle) flashing to 580 K. Clearly, component II assigned to the OH groups decrease in intensity upon flashing, while component I assigned to FeO(111) and component IV assigned to surface FeO_2 without OH groups increase in intensity. Further, we note that the FeO_2 interface component decreases in intensity. This is as expected because part of the surface is converted to FeO(111) without an interface component. Hence, flashing in vacuum leads to removal of the hydrogen, as expected, and a partial removal of oxygen leads to the observed trilayer/bilayer mixture. This observation suggests that OH groups help to stabilize the FeO_2 trilayer. Recently, it has been reported by Liu et al. [42] that hydroxyl groups also stabilize ultrathin Zinc oxide films.

The topmost O 1s spectrum in Fig. 2 was acquired after a subsequent room temperature exposure of H_2O

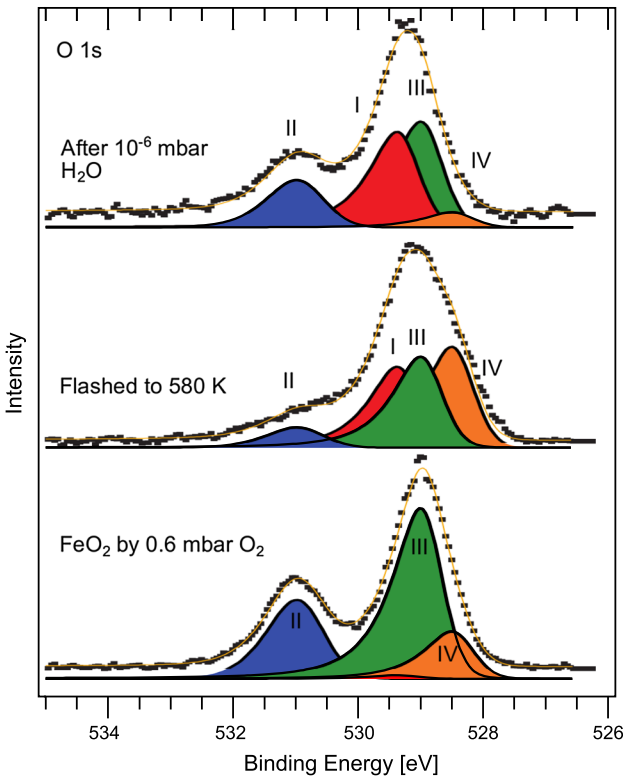

Fig. 2 O 1s spectra of FeO_2(111) before (*bottom*) and after (*middle*) flashing to 580 K. The spectra at the *top* was acquired after exposing the flashed FeO_2(111) film to 1×10^{-6} mbar H_2O for $\sim$15 min

(1×10^{-6} mbar for $\sim$15 minutes) onto this trilayer/bilayer mixture. Clearly, the water exposure leads to re-appearance of the OH-component (II) and a reduced FeO_2 surface component (IV). In contrast, the FeO(111) component (I) and the FeO_2 interface component (III) are unaffected by the water exposure. Hence, the conclusion from these observations is that a surface with FeO_2(111) patches effectively dissociates H_2O, whereas a continuous FeO(111) film is inert with respect to water exposure at room temperature.

For the oxidation of FeO(111) to FeO_2 discussed above a pressure of 0.6 mbar was used. At such high pressures—high as in orders of magnitudes higher than standard UHV techniques—it is difficult to avoid water impurities. In order to reduce the water contamination we also studied the oxidation of FeO(111) by NO_2. Previous surface oxidation studies have shown that NO_2 functions as a very efficient oxidation agent and quite similar to atomic oxygen [43], meaning that the partial pressure of water can be reduced significantly. Figure 3 show a series of O 1s spectra of FeO(111) exposed to an increasing amount of NO_2 dosed at room temperature. As the gas dosing was done in the preparation chamber the sample was transferred between dosing and measurement. After 250 L NO_2 (dosed at

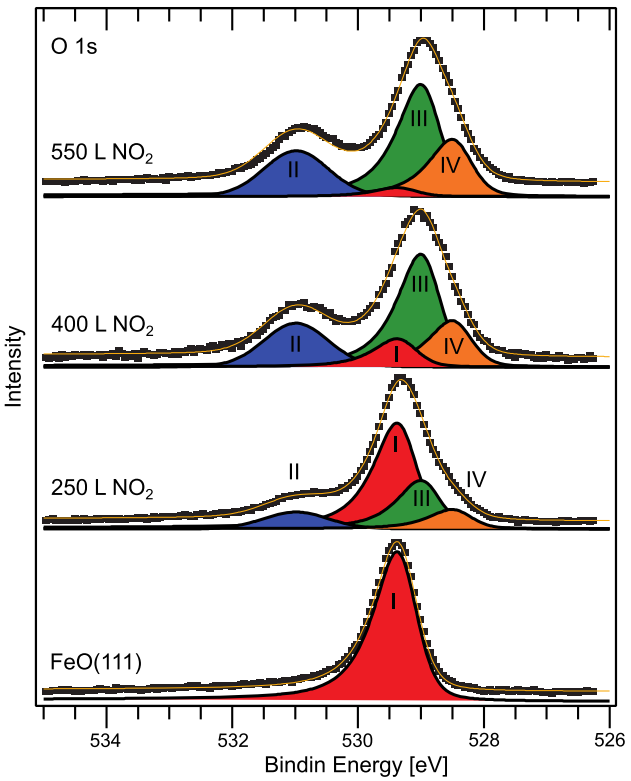

Fig. 3 Trilayer FeO_2 grown with NO_2. The *bottom* spectrum shows bilayer FeO(111) and each spectrum above shows the spectrum after subsequent room temperature NO_2 dosing. Dose shown in the figure is the cumulative NO_2 dose

1×10^{-6} mbar) the OH component (II), the FeO_2 surface component (IV), and the FeO_2 interface component (III) start to become visible. At lower NO_2 doses (not shown) the spectrum looked very similar to that of pristine FeO(111) and only very small changes were observed. With increasing NO_2 dose the components assigned to FeO_2 (II, III, IV) increase in intensity while the FeO(111) component (I) decreases. Between a dose of 400 and 550 L the surface oxidation seems to saturate and the FeO(111) component (I) almost disappears. No N 1s signal was observed upon NO_2 oxidation in any of our experiments suggesting formation of NO or N_2 that immediately desorbs. Comparing the O 1s spectra after O_2 oxidation (Fig. 1a) and the NO_2 oxidation (Fig. 3) of FeO(111) it is evident that the two different oxidation methods are very similar and both result in extensive surface hydroxylation. In none of our NO_2 oxidation experiments we observed FeO_2 interface (II) and surface (IV) components without also observing a OH component (IV). Altogether, these observations suggest that a surface with FeO_2(111) trilayer patches undergoes quickly hydroxylation, whereas the bilayer FeO(111) film does not hydroxylate.

3.3 STM Comparison of FeO and FeO_2

Evidence for spontaneous hydroxylation of the FeO_2 trilayer is also provided by STM measurements. Figure 4 shows STM images of the pristine bilayer FeO film (Fig. 4a) and the oxidized film (Fig. 4b), produced by exposure to atomic oxygen from a thermal cracker. Immediately after exposure at room temperature, it was found to be impossible to establish stable STM imaging, presumably due to the presence of weakly-bound oxygen-containing species on the surface which interact strongly with the STM tip. After flashing the surface to 500 K, however, stable images could be obtained, one of which is shown in Fig. 4b. Similar to previous reports [23, 26, 35], the STM images show bright patches of FeO_2 organized following the moiré superstructure. Atop these patches we observe bright protrusions showing poor short-range order, but typical separations corresponding to $\sqrt{3} \times$ a, or next-nearest-neighbor spacing or larger. This is very similar to what has previously been observed for H adatoms adsorbed on the FeO bilayer [22], and we therefore propose that these protrusions correspond to OH groups which are either residual features following the flash (note that the OH component of the O 1s spectra shown above was not completely removed by heating) or which formed by adsorption while the sample cooled. To distinguish between these two possibilities, it would be interesting to scan on FeO_2 trilayer samples at elevated temperatures. The unintentional adsorption of water upon sample cooling was previously observed in STM studies addressing rutile TiO_2(110) [44]. In an earlier report by Giordano et al. [26] protrusions were observed in STM images similar to those here, but forming a more well-ordered $\sqrt{3} \times \sqrt{3}R30^\circ$ arrangement atop the trilayer patches. In that work the superstructure was attributed to outward relaxation of 1/3 of the Fe ions based on the finding by DFT+U calculations that such a structure was stable. Though we cannot rule out this explanation completely, we find it unlikely that displacement of single ions is responsible for the protrusions observed in the present case, where variability in the number of protrusions observed at each FeO_2(111) patch and their relatively random ordering is suggestive of the presence of foreign species. We furthermore suggest that the superstructure observed in this previous work was also caused by OH groups, the better ordering being attributable to a higher concentration of these species.

3.4 XAS Comparison of FeO and FeO_2

We now take a closer look at the oxidation state of Fe in FeO(111) and FeO_2. In Fig. 5 Fe L_3 spectra of a FeO(111) film and FeO_2 prepared by dosing NO_2 are shown together

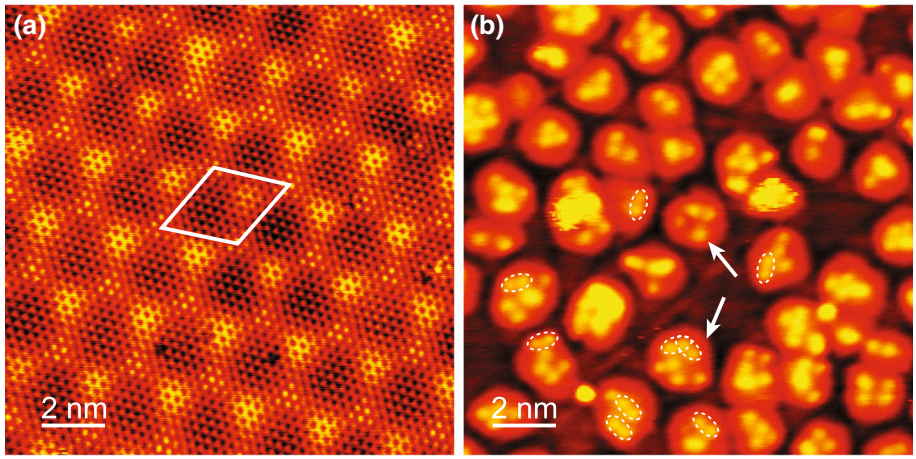

Fig. 4 **a** STM image (65 mV, 3.0 nA) of bilayer FeO/Pt(111), with the moiré coincidence cell marked. **b** STM image (2.0 V, 0.2 nA) of the FeO bilayer following exposure to atomic oxygen and flashing to 500 K. Bright protrusions assigned to OH groups incorporated into patches of the FeO_2 trilayer are indicated with arrows. *Ovals* mark pairs of protrusions separated by a lattice distance of $\sqrt{3}$

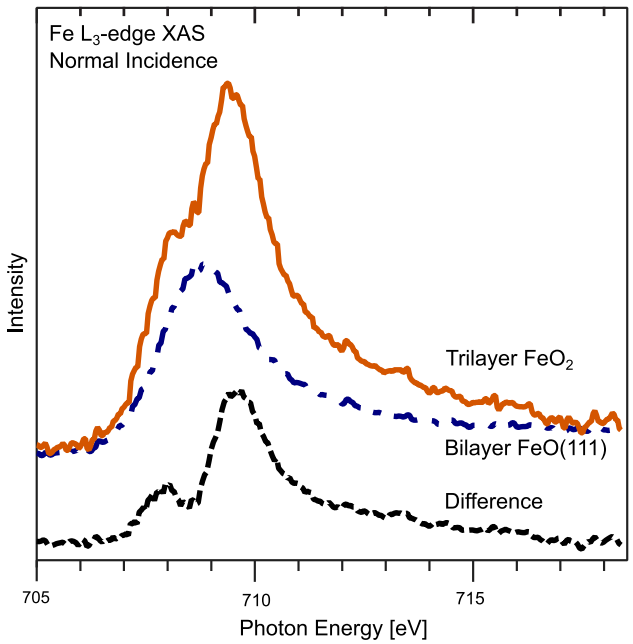

Fig. 5 Normal incidence Fe L_3-edge XAS spectra of a trilayer grown with NO_2 and a bilayer, from which the trilayer was grown. Also shown is the difference between the spectra

with their difference spectra. The spectrum of the FeO(111) bilayer film is, as expected, in accordance with that of Fe^{2+} [5, 45, 46]. For FeO_2 the main component is shifted to higher photon energies and a shoulder is seen at a lower photon energy. Clearly, the iron atoms in FeO_2 are at least partly in a different oxidation state. Indeed, the observed line-shape of the difference spectrum [FeO_2–FeO(111)] is characteristic of an Fe^{3+} oxidation state [45, 46]. Hence, the trilayer is composed of Fe^{2+} and Fe^{3+} contributions. From the relative intensities of the contributions we find that roughly 60 % of the ions are in an Fe^{2+} oxidation state. As previously discussed, no bilayer FeO(111) contributions could be found with XPS. Therefore, the different Fe ion oxidation state must originate from the trilayer FeO_2 patches.

3.5 In Situ Oxidation of FeO to FeO_2 Followed with APXPS

In all our experiments where FeO(111) was oxidized to FeO_2 with O_2, NO_2, and atomic oxygen we observed that the surface is to a large extent hydroxylated. To follow the kinetics of the FeO(111) to FeO_2 transformation and to probe whether the surface first is oxidized to FeO_2 and subsequently becomes hydroxylated we followed the oxidation process in situ with APXPS. In the APXPS experiment the FeO(111) surface was exposed to 0.6 mbar O_2 while the sample temperature was ramped from room temperature to 500 K (Fig. 6). At the same time O 1s XP spectra were measured. Figure 6a shows an image plot of the O 1s spectra acquired in situ while selected O 1s spectra are shown in panel (b). The doublet observed near 538 eV originates from the O_2 gas phase molecules and the peaks near 530 eV originate from surface O species. In the top part of panel (c) in Fig. 6 we plot the relative surface area of all O 1s surface components obtained from simultaneous curve fitting of all O 1s spectra acquired in situ. At 300 K the surface is completely covered by bilayer FeO(111) (I). At a temperature of 315 K after $\sim$20 min of O_2 exposure we observe the onset of the reduction of FeO(111) component (I) and the simultaneous increase of the FeO_2-OH component (II) and the FeO_2 (IV) component. Thus, the FeO_2 surface atoms with and without adsorbed H occurs simultaneously and both components grow with the same rate until a temperature of 360 K is reached. Above this temperature the FeO_2-surface component start to increase faster than the FeO_2-OH component, and above 400 K the OH coverage reaches maximum (33 %) and start to decrease at higher temperatures. Both observations suggest

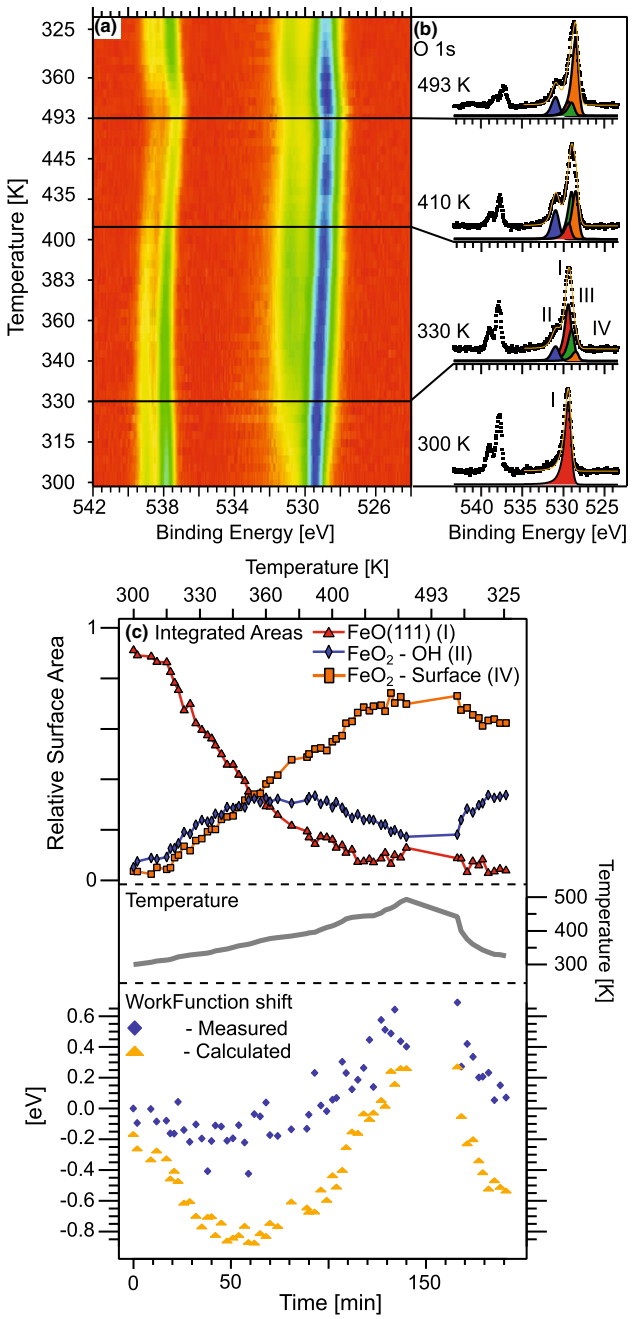

Fig. 6 **a** Image plot of O 1s spectra acquired in 0.6 mbar O_2 while heating the sample from 300 to 500 K followed by subsequent cooling. The temperature profile is plotted in *panel c*. **b** Selected O 1s spectra from *a*. **c** *Top* development of the 3 surface components [FeO(111)(I), FeO_2-OH(II), and FeO_2-Surface (IV)] as function of temperature and exposure time obtained from curve fitting the O 1s spectra shown in *panel a*. *Bottom* measured work function shift as function of temperature and exposure time obtained from the energy shift of the O_2 gas phase peak plotted together with the calculated workfunction shift obtained by combining theoretical values from ref. [29] and the coverage of FeO_2-OH(II) and FeO_2-Surface(IV)

that hydroxylation is suppressed at higher temperature. Even though the OH formation is suppressed at higher temperature we always observe a significant degree of hydroxylation also at the maximum temperature of 500 K (20 %). Upon cooling the OH coverage increase again and the FeO_2-surface component decrease.

Finally, we take a look at the peak position of the O_2 gas phase doublet. In contrast to the O 1s surface atoms that are pinned to the Fermi level the gas phase molecules are pinned to the vacuum level. As a result, the binding energy of gas phase molecules follows surface work function shift during the reaction, in this case, the film growth [47]. It should, however, be kept in mind that the gas phase molecules probed by APXPS are located in a small volume between the sample surface and the grounded electron analyzer aperture. Therefore, the measured binding energy shift of the gas phase molecules is reduced as compared to the work function shift of the sample surface. Nevertheless, at the bottom of Fig. 6c we plot the work function change obtained from the peak position of the O_2 doublet as function of time and temperature. In ref. [29] Giordano et al. calculated the work function change relative to Pt(111) of FeO(111) (+0.31 eV), FeO_2 (+1.72 eV), and FeOOH (-3.89 eV). Using these values and the relative surface coverage of the same components from the top part of Fig. 6c we estimated the expected work function shifts as the FeO(111) film is oxidized and hydroxylated as $\Delta\phi = \Theta(FeO_2 - surface) \cdot 1.41\ \text{eV} - \Theta(FeO_2 - OH) \cdot 4.20\ \text{eV}$. As Fig. 6c demonstrates the estimated work function qualitatively reproduce the measured work function rather well keeping in mind the simplicity of our model and the error bars of the curve fitting. In addition, we note that the calculated work function shift for FeOOH (−3.89 eV) probably overestimates the work function shift in our case, because it was calculated for a full OH coverage, leading to vertical configuration of all OH groups. In our case with partial hydroxylation of the FeO_2, the OH groups are dynamically distorted leading to a reduced effective dipole moment. Altogether we conclude from the data presented in Fig. 6c that: (i) the onset of hydroxylation coincides with the onset of the FeO_2 formation and initially the OH coverage and the FeO_2 formation grows simultaneously, meaning that OH formation is closely connected to the trilayer structure and/or growth; (ii) the degree of hydroxylation is strongly temperature dependent; (iii) the O atoms in the FeO_2 patches are always only partly covered with H atoms, in agreement with our STM observations; (iv) the FeO_2 formation and hydroxylation lead to a measurable work function shift that fits well with our

assignment of the the O 1s components and the calculated work function differences between FeO_2, hydroxylated FeO_2, and FeO(111).

As discussed above, the onset of hydroxylation coincides with the onset of FeO_2 formation, suggesting that hydroxylation occurs during the formation of the FeO_2 trilayer rather than after its formation is completed. On this basis and the fact that hydroxylation also occurred after the formation of FeO_2 patches was completed (see Fig. 2c) we suggest that water dissociates at the FeO_2-FeO(111) interface and at defects that are present mainly during the oxidation process. In contrast, we do not expect that water dissociates on perfect continuous FeO(111) films and on the FeO_2 patches.

Previous studies have shown that FeO bilayer films can be grown also on other Pt facets [48], and many other single-crystalline metal substrates such as Pd(111) [35], Ag(100) [41], Ag(111) [49], Mo(100) [50], Ru(0001) [51] and Au(111) [52, 53]. In other studies it has been found that FeO(111) films encapsulate Fe_3O_4 supported Pt particles [54]. In addition, it has been demonstrated recently that Co–O bilayer films on Au(111) can be transformed to O–Co–O trilayer films , both of which are structurally very similar to the iron oxide phases discussed here [55]. Our finding that the Pt(111) supported FeO_2 trilayer films are generally hydroxylated could thus be relevant both for surface iron oxides on other supports and for other trilayer surface oxides on (111) noble metal surfaces.

4 Conclusions

To conclude, we monitored the FeO(111)/Pt(111) to FeO_2/Pt(111) conversion upon oxidation with different oxidizing agents with HRXPS and APXPS and provided spectroscopic fingerprints of these surface iron oxide phases. Most importantly, we showed that FeO_2 supported by Pt(111) is very active for water dissociation. Once FeO_2 trilayer patches are formed upon oxidation of bilayer FeO(111) films with O_2, NO_2, or atomic oxygen, they immediately become partly hydroxylated. Since we always observe a significant degree of hydroxylation also when FeO(111) is oxidized to FeO_2 at excellent UHV conditions and since our STM data of the hydroxylad FeO_2 patches looks almost identical to previously published STM images of FeO_2 [23, 26] we propose that catalytically highly active FeO_2 trilayer films are generally hydroxylated even at normal UHV conditions. We believe this result is also of relevance for iron oxide films on other supports and for other trilayer oxides grown on (111) noble metal surfaces.

Acknowledgments Financial support from Vetenskapsrådet (Grants Nos. 2010-5080 and 2012-3850) and assistance by the staff at the MAX IV Laboratory are gratefully acknowledged. The work in Aarhus was supported by the Villum Kahn Rasmussen Foundation.

References

1. Surnev S, Fortunelli A, Netzer FP (2013) Chem Rev 113:4314
2. Vurens GH, Salmeron M, Somorjai GA (1988) Surf Sci 201:129
3. Ritter M, Ranke W, Weiss W (1998) Phys Rev B 57:7240
4. Ranke W, Ritter M, Weiss W (1999) Phys Rev B 60:1527
5. Weiss W, Ranke W (2002) Prog Surf Sci 70:1
6. Rienks EDL, Nilius N, Rust HP, Freund HJ (2005) Phys Rev B 71:241404
7. Merte LR, Grabow LC, Peng G, Knudsen J, Zeuthen H, Kudernatsch W, Porsgaard S, Laegsgaard E, Mavrikakis M, Besenbacher F (2011) Jour Phys Chem C 115:2089
8. Kim YJ, Westphal C, Ynzunza RX, Galloway HC, Salmeron M, Van Hove MA, Fadley CS (1997) Phys Rev B 55:R13448
9. Zhang W, Li Z, Luo Y, Yang J (2009) Jour Phys Chem C 113:8302
10. Giordano L, Pacchioni G, Goniakowski J, Nilius N, Rienks EDL, Freund HJ (2007) Phys Rev B 76:075416
11. Huang W, Ranke W (2006) Surf Sci 600:793
12. Merte LR, Knudsen J, Grabow LC, Vang RT, Laegsgaard E, Mavrikakis M, Besenbacher F (2009) Surf Sci 603:L15
13. Knudsen J, Merte LR, Grabow LC, Eichhorn FM, Porsgaard S, Zeuthen H, Vang RT, Laegsgaard E, Mavrikakis M, Besenbacher F (2010) Surf Sci 604:11
14. Merte LR, Knudsen J, Eichhorn FM, Porsgaard S, Zeuthen H, Grabow LC, Laegsgaard E, Bluhm H, Salmeron M, Mavrikakis M, Besenbacher F (2011) J Am Chem Soc 133:10692
15. Nilius N, Rienks EDL, Rust HP, Freund HJ (2005) Phys Rev Lett 95:066101
16. Giordano L, Pacchioni G, Goniakowski J, Nilius N, Rienks EDL, Freund HJ (2008) Phys Rev Lett 101:026102
17. Berdunov M, Mariotto G, Balakrishnan K, Murphy S, Shvets IV (2006) Surf Sci 600:L287
18. Lin X, Nilius N (2008) J Phys Chem C 112:15325
19. Joseph Y, Ranke W, Weiss W (2000) J Phys Chem B 104:3224
20. Leist U, Ranke W, Al-Shamery K (2003) Phys Chem Chem Phys 5:2435
21. Merte LR, Peng C, Bechstein R, Rieboldt F, Farberow CA, Grabow LC, Kudernatsch W, Wendt S, Laegsgaard E, Mavrikakis M, Besenbacher F (2012) Science 336:889
22. Merte LR, Bechstein R, Peng G, Rieboldt F, Farberow CA, Zeuthen H, Knudsen J, Laegsgaard E, Wendt S, Mavrikakis M, Besenbacher F (2014) Nat Commun 5:4193
23. Sun YN, Qin ZH, Lewandowski M, Carrasco E, Sterrer M, Shaikhutdinov S, Freund H (2009) J Catal 266:359
24. Fu Q, Li WX, Yao Y, Liu H, Su HY, Ma D, Gu XQ, Chen L, Wang Z, Zhang H, Wang B, Bao X (2010) Science 328:1141
25. Sun YN, Giordano L, Goniakowski J, Lewandowski M, Qin ZH, Noguera C, Shaikhutdinov S, Pacchioni G, Freund HJ (2010) Angew Chem Int Ed 49:4418
26. Giordano L, Lewandowski M, Groot IMN, Sun YN, Goniakowski J, Noguera C, Shaikhutdinov S, Pacchioni G, Freund HJ (2010) J Phys Chem C 114:21504
27. Lewandowski M, Sun YN, Qin ZH, Shaikhutdinov S, Freund HJ (2011) Appl Catal A 391:407
28. Lewandowski M, Groot IMN, Shaikhutdinov S, Freund HJ (2012) Catal Today 181:52
29. Giordano L, Pacchioni G, Noguera C, Goniakowski J (2013) Top Catal 56:1074
30. Giordano L, Pacchioni G, Noguera C, Goniakowski J (2014) ChemCatChem 6:185

31. Ringleb F, Fujimori Y, Wang HF, Ariga H, Carrasco E, Sterrer M, Freund HJ, Giordano L, Pacchioni G, Goniakowski J (2011) J Phys Chem C 115:19328
32. Nyholm R, Andersen JN, Johansson U, Jensen BN, Lindau I (2001) Nucl Instrum Methods A 467:520
33. Schnadt J, Knudsen J, Andersen JN, Siegbahn H, Pietzsch A, Hennies F, Johansson N, Mårtensson N, Öhrwall G, Bahr S, Mähl S, Schaff O (2012) J Synchotron Radiat 19:701
34. Denecke R, Väterlein P, Bässler M, Wassdahl N, Butorin S, Nilsson A, Rubensson JE, Nordgren J, Mårtensson N, Nyholm R (1999) J Electron Spectro Relat Phenom 101:971
35. Zeuthen H, Kudernatsch W, Peng G, Merte LR, Ono LK, Lammich L, Bai Y, Grabow LC, Mavrikakis M, Wendt S, Besenbacher F (2013) J Phys Chem C 117:15155
36. Björneholm O, Nilsson A, Tillborg H, Bennich P, Sandell A, Hernnäs B, Puglia C, Mårtensson N (1994) Surf Sci 315:L983
37. Joseph Y, Kuhrs C, Ranke W, Ritter M, Weiss W (1999) Chem Phys Lett 314:195
38. Liu P, Kendelewicz T, Brown GE, Nelson EJ, Chambers SA (1998) Surf Sci 417:53
39. Sirotti F, Rossi G (1994) Phys Rev B 49:15682
40. McIntyre NS, Zetaruk DG (1977) Anal Chem 49:1521
41. Merte LR, Shipilin M, Ataran S, Blomberg S, Zhang C, Mikkelsen A, Gustafson J, Lundgren E (2015) J Phys Chem C 119:2572
42. Liu BH, Boscoboinik JA, Cui Y, Shaikhutdinov S, Freund HJ (2015) J Phys Chem C 119:7842
43. Schnadt J, Knudsen J, Hu XL, Michaelides A, Vang RT, Reuter K, Li Z, Lægsgaard E, Scheffler M, Besenbacher F (2009) Phys Rev B 80:075424
44. Wendt S, Schaub R, Matthiesen J, Vestergaard EK, Wahlström E, Rasmussen MD, Thostrup P, Molina LM, Laegsgaard E, Stensgaard I, Hammer B, Besenbacher F (2005) Surf Sci 598:226
45. Laan GVD, Kirkman IW (1992) J Phys Condens Matter 4:4189
46. Cressey G, Henderson CMB, Laan GVD (1993) Phys Chem Miner 20:111
47. Bluhm H (2010) J Electron Spectrosc Relat Phenom 177:71
48. Shaikhutdinov S, Ritter M, Weiss W (2000) Phys Rev B 62:7535
49. Waddill GD, Ozturk O (2005) Surf Sci 575:35
50. Corneille JS, He JW, Goodman DW (1995) Surf Sci 338:211
51. Ketteler G, Ranke W (2003) J Phys Chem B 107:4320
52. Khan NA, Matranga C (2008) Surf Sci 602:93
53. Deng X, Lee J, Wang C, Matranga C, Aksoy F, Liu Z (2011) Langmuir 27:2146
54. Qin ZH, Lewandowski M, Sun YN, Shaikhutdinov S, Freund HJ (2008) J Phys Chem C 112:10209
55. Walton AS, Fester J, Bajdich M, Arman MA, Osiecki J, Knudsen J, Vojvodic A, Lauritsen JV (2015) ACS Nano 9:2445